buildings

MDPI

Article

Research on the Configuration of Multi-Component Solid Waste Cementitious Materials and the Strength Characteristics of Consolidated Aeolian Sand

Akelamjiang Maimait [1,2], Yaqiang Wang [1], Jianjun Cheng [1,*], Yanfu Duan [1] and Zhouyang Pan [1]

[1] College of Water Resources and Architectural Engineering, Shihezi University, Shihezi 832003, China; akelamjiang@stu.shzu.edu.cn (A.M.); wangyaqiang@stu.shzu.edu.cn (Y.W.); lttdyf@163.com (Y.D.); 20242110003@stu.shzu.edu.cn (Z.P.)
[2] Xinjiang Kusha Highway Development Co., Ltd., Aksu 842202, China
* Correspondence: chengjianjun@shzu.edu.cn

Abstract: Developing green, low-carbon building materials has become a viable option for managing bulk industrial solid waste. This paper presents a kind of all solid waste cementitious material (SWCM), which is made entirely from six common industrial wastes, including carbide slag and silica fume, that demonstrate strong mechanical properties and effectively stabilize aeolian sand (AS). Initially, we investigated the mechanical strength of waste-based cementitious materials in various mix ratios, focusing on their ability to stabilize river sand (RS) and aeolian sand. The results show that it is necessary to use alkaline solid waste carbide slag to provide a suitable reaction environment to achieve the desired strength. In contrast, the low reactivity of coal gangue powder did not contribute effectively to the strength of the cementitious material. Further orthogonal experiments determined the impact of different waste dosages on the strength of stabilized AS. It was found that increasing the amounts of carbide slag, silica fume, and blast furnace slag powder improved strength, while increasing fly ash first increased and then decreased strength. In contrast, higher additions of desulfurization gypsum and coal gangue powder led to a continuous decrease in strength. The optimized mix is carbide slag—desulfurization gypsum—fly ash—silica fume—blast furnace slag powder in a ratio of 4:2:2:3:3. The experimental results using SWCM to stabilize AS indicated a proportional relationship between strength and SWCM content. When the content is $\geq$20%, it meets the strength requirements for road subbases. The primary hydration products of stabilized AS are C-(A)-S-H, AFt, and $CaCO_3$. Increasing the SWCM content enhances the reaction degree of the materials, thereby improving mechanical strength. This study highlights the mechanical properties of cementitious materials made entirely from waste for stabilizing AS. It provides a reference for the large-scale utilization of industrial solid waste and practical applications in desert road construction.

Keywords: bulk industrial solid waste; cementitious material; aeolian sand; strength characteristics

Citation: Maimait, A.; Wang, Y.; Cheng, J.; Duan, Y.; Pan, Z. Research on the Configuration of Multi-Component Solid Waste Cementitious Materials and the Strength Characteristics of Consolidated Aeolian Sand. *Buildings* **2024**, *14*, 3059. https://doi.org/10.3390/buildings14103059

Academic Editor: Rui Xiao

Received: 3 September 2024
Revised: 18 September 2024
Accepted: 20 September 2024
Published: 25 September 2024

1. Introduction

In a highly modernized industrial system, the increasing volume of bulk industrial solid waste poses significant environmental challenges. Addressing and utilizing this waste has become a critical factor in sustainable development, necessitating more scientific and effective measures across various industries. Using bulk industrial solid waste in building materials, particularly in engineering applications, is an effective way to utilize resources. This approach helps address waste disposal issues, alleviates shortages of construction minerals, reduces building costs, and contributes to green and sustainable development. Cementitious materials made from industrial solid waste are a hot research topic in the field of environmental materials, with significant progress already made. These waste-based cementitious materials exhibit excellent mechanical properties, durability, and environmental benefits, making them suitable for a wide range of construction applications.

In terms of raw material ratios, suitable materials can be combined based on the composition and properties of the waste. Alkaline wastes, which provide a favorable reaction environment, are widely used in the preparation of cementitious materials. For example, significant research has been conducted on red mud-based environmentally friendly cementitious materials [1]. Garanayak et al. [2] studied the application of varying proportions of granulated slag and red mud in cementitious materials, finding that alkaline red mud is suitable for their preparation. Zhu et al. [3] used various wastes and cement to produce red mud-based cementitious materials, discovering that the main hydration products include calcium silicate hydrate, tobermorite, and $Ca(OH)_2$. Other alkaline wastes, such as carbide slag and steel slag, have also been extensively studied. Ren et al. [4] prepared composite cementitious materials using aluminum slag, carbide slag, coal gangue, and magnesium desulfurization slag, finding that these materials have better mechanical properties and water resistance than conventional magnesium-potassium phosphate cement. Zhang et al. [5] used carbide slag and other stabilizing materials to produce cementitious materials. Research by Carvalho et al. [6] demonstrated that steel slag powder can enhance the mechanical performance of cement-based composite materials. Wang et al. [7] explored the engineering properties of composite cementitious materials made with steel slag powder and rice husk ash, finding that their freeze resistance and durability exceed those of pure cement. Due to its excellent physicochemical properties, fly ash not only serves as a partial substitute for cement, but also constitutes a pivotal raw material in the production of composite cementitious materials [8]. The incorporation of fly ash under certain conditions can effectively enhance both the workability and mechanical properties of the resulting paste [9,10]. Sulfates generated from the sulfate ions in gypsum-based wastes can improve mechanical properties, making them a common additive. Wang et al. [11] developed cementitious materials using fly ash, desulfurization gypsum, and shell powder, showing that these materials meet the performance requirements of ordinary Portland cement. Yang et al. [12] studied modified magnesium slag, gasification slag, and desulfurization gypsum cementitious materials, finding that they can effectively stabilize coal gangue and meet initial requirements for mine backfilling. Liu et al. [13] prepared composite cementitious materials using desulfurization gypsum, fly ash, granulated blast furnace slag, and cement, showing that desulfurization gypsum and cement can react synergistically to enhance mechanical performance. Further research indicates significant progress in cementitious materials made from alkaline wastes and key components such as desulfurization gypsum. Wang et al. [14] studied cementitious materials made from red mud, desulfurization gypsum, and fly ash, finding that the synergistic effect of alkaline red mud and sulfates can activate silica-alumina oxides to produce mineral gels, with 28-day strength reaching 50.6 MPa at a 50% replacement level. Wu et al. [15] prepared cementitious materials using a combination of red mud, fly ash, desulfurization gypsum, and blast furnace slag powder, showing that the system's aluminosilicate minerals can effectively replace some cement clinker through alkali and sulfate activation. Tang et al. [16] used refined slag, blast furnace slag powder, steel slag, and desulfurization gypsum to create filling cementitious materials, demonstrating that adding refined slag increases the content of alumina silicate and accelerates the hydration reaction. Wu et al. [17] found that slag, steel slag, and desulfurization gypsum-based cementitious materials show good early crack resistance when stabilizing gravel. Gu et al. [18] prepared paste-like cementitious materials using phosphogypsum, finding that the water-to-binder ratio and phosphogypsum content positively affect setting time and flowability, with the addition of cement and silica fume enhancing strength and water stability. Xue et al. [19] investigated the synthesis of cementitious materials from electrolytic manganese slag combined with granulated blast furnace slag, clinker, and lime, showing that this method can effectively immobilize heavy metals in electrolytic manganese slag.

In terms of preparation processes, improving raw material reactivity can be achieved by adjusting process parameters and applying new preparation technologies. Zhao et al. [20] noted that wet-milling coal gangue can alter its crystal structure, enhancing reactivity and

making it an effective supplementary material for cementitious materials. Additionally, extending the milling time increases reactivity of the coal gangue and the likelihood of dihydroxylation [21]. Jiang et al. [22] used hemihydrate phosphogypsum to prepare filling binders, showing that the addition of quicklime can shorten setting time and improve early strength. After adding tailings, the compressive strength meets the requirements for mine backfilling. Gu et al. [23] studied the stabilization of loess using cement, phosphogypsum, fly ash, and quicklime, finding that curing temperature can improve soil strength and accelerate the formation of hydration products. Wu et al. [24] used thermal activation to process construction demolition waste, effectively promoting the hydration reaction of cementitious materials. Shi et al. [25] investigated the effects of carbon-to-oxygen ratio, alkalinity range, and temperature on the reduction of iron in lignite and the production of cementitious materials, finding that the optimal carbon-to-oxygen ratio is 1.2, the alkalinity range is 2.4–3.3, the reduction temperature is $\leq$1137 °C, and the production temperature is 1450 °C. Shi et al. [26] discussed the feasibility of simultaneously producing nickel–iron and cementitious materials under various thermal conditions, highlighting that the complete reduction of iron is essential for the generation of C3S. Zhao et al. [27] showed that incineration fly ash treated by molten salt processes exhibits good cementitious properties. Mao et al. [28] prepared cementitious materials using water-washed municipal solid waste incineration fly ash (MSWI-FA), flue gas desulfurization gypsum, and aluminum ash. They demonstrated that water washing effectively removes chloride salts, and MSWI-FA can contribute to the production of sulfate–aluminate-based cementitious materials.

In terms of modification methods, selecting appropriate additives to provide physical or chemical enhancement is an important research direction for improving the performance of cementitious materials. NaOH, a commonly used alkaline activator, was employed by Su et al. [29] to activate fly ash, red mud, recycled fines, brick powder, coal gangue powder, and cement kiln dust. They found that NaOH concentration, water-to-binder ratio, and curing humidity affect the strength of each material to varying degrees. A Na_2SiO_3 solution is also commonly used for modification. Alam et al. [30] studied the effect of a Na_2SiO_3 solution on the strength and durability of granulated blast furnace slag stabilizing red mud. They found that alkali activation results in higher impact strength and wet–dry cycle durability. Further research involves combining multiple alkaline solutions or adding active oxides as activators. Burciaga-Díaz et al. [31] reported that using a 1:1 MgO-NaOH composite activator effectively activates blast furnace slag, resulting in better mechanical performance compared to single activators. Puertas et al. [32] investigated the activation of blast furnace slag using solutions of water glass, NaOH/Na_2CO_3 mixtures, and waste glass dissolved in NaOH/Na_2CO_3. They found that the combination of waste glass and alkaline solutions effectively activates blast furnace slag, with mechanical strength and microstructural development comparable to conventional activation results. Dung et al. [33] used active MgO and Na_2CO_3 to activate granulated blast furnace slag, showing that these agents accelerate slag dissolution, shorten setting time, and enhance mechanical strength. Chen et al. [34] used calcium carbide residue and Na_2CO_3 to activate waste glass powder, finding that replacing some fly ash with waste glass powder promotes alkali activation reactions in fly ash and blast furnace slag systems, reducing fluidity and improving mechanical strength. Research on other modification methods, such as Shen et al. [35] analysis, indicates that the water-to-binder ratio has the greatest impact on the shrinkage performance of alkali-activated slag–fly ash geopolymers, while the silica–alumina ratio most affects mortar shrinkage. Zanotti et al. [36] explored the suitability of using geopolymers as a cement substitute, showing that adding fibers can increase cohesiveness and improve crack resistance at interfaces. Kianynejad et al. [37] incorporated glass wool residue fibers into carbide slag and metakaolin-stabilized poorly graded sandy soils, showing that adding fibers improves the mechanical performance of the system and alters the failure mode.

In summary, research on cementitious materials made from bulk industrial solid waste has made notable progress, but several challenges remain. The complexity and variability

of waste composition and properties make stability difficult to control. High-performance waste-based cementitious materials often require chemical additives, raising concerns about cost and environmental safety. Considering the high environmental compatibility of industrial waste road materials, existing studies show that common large-scale industrial wastes used as road materials can meet environmental standards [38,39]. Additionally, solid waste binders can act as curing and encapsulating agents, fixing harmful substances and heavy metals [40–42]. Given the varying mechanical strength requirements for different road grades and structural layers, fully solid waste-based cementitious materials for road construction have significant potential applications. Therefore, this paper explores the recipe for preparing fully sold waste-based cementitious materials (SWCM). It also addresses the extensive demand for stabilized AS in desert engineering. By investigating the strength characteristics of fully waste-based cementitious materials in stabilizing AS, the study aims to determine the optimal waste mix and understand the material mechanisms, providing valuable references for future research and application.

2. Materials and Experimental Methods

2.1. Raw Test Materials

This study uses aeolian sand (AS) and river sand (RS) as fine aggregates, and the waste materials include coal gangue (CG) powder, fly ash (FA), silica fume (SF), desulfurization gypsum (DG), blast furnace slag powder (BFS), and carbide slag (CS). RS and the six types of waste materials were sourced from the Shihezi area in Xinjiang, while the AS was obtained from Kuqa in Xinjiang. The theoretical maximum dry densities of these materials are shown in Table 1. The particle size distribution of the AS is illustrated in Figure 1, which shows that the main particle size ranges from 0.075 to 0.25 mm, comprising 72.69% of the total, with 7.21% of particles smaller than 0.075 mm, and 18.43% in the 0.25 to 0.5 mm range, indicating a concentrated distribution. The RS primarily has a particle size distribution between 0.1 and 2 mm, with a fineness modulus of 2.11, classifying it as fine sand.

Table 1. Theoretical maximum dry density of test materials.

Materials	AS	CG	FA	SF	DG	BFS	CS
Density (g/cm^3)	2.63	2.84	2.59	2.26	2.84	3.02	2.45

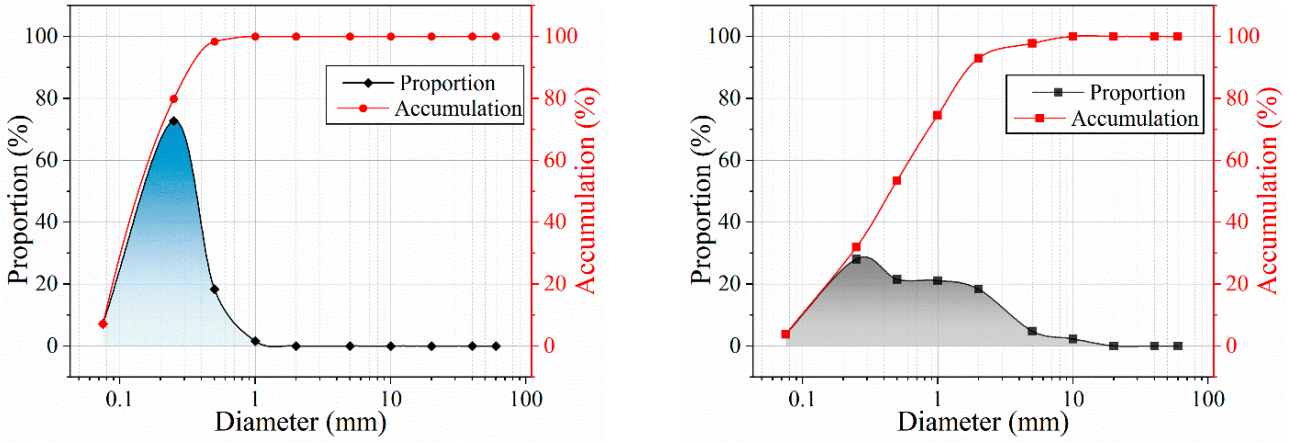

(**a**) AS (**b**) RS

Figure 1. Sand particle size distribution curve.

All six waste materials are in powder form, with primary particle sizes smaller than 0.075 mm. The microscopic morphology and main chemical compositions of each waste material are shown in Figure 2 and Table 2. Figure 2a shows that coal gangue powder has irregular particles with smooth surfaces, a particle size distribution between 5 and 30 μm,

good dispersion, and a white color. Its main chemical components are SiO_2, CaO, and Al_2O_3. Figure 2b shows that fly ash particles are spherical, with crystal fragments attached to their surfaces. The particle size distribution is concentrated between 1 and 5 μm, exhibiting good flowability, and its color is gray. The main chemical elements are SiO_2 and Al_2O_3. Figure 2c shows that silica fume particles are also spherical but smaller, with a primary size between 0.1 and 0.2 μm. They exhibit strong agglomeration due to matrix suction, forming tight clusters. The primary chemical component is SiO_2, and the fume contains 29.64% carbon, giving it a dark gray appearance. Figure 2d shows that desulfurization gypsum particles are irregular, with some resembling cubes. They are larger, with a primary size between 20 and 60 μm, have a grayish-white color, and moderate dispersion. The main chemical component is $CaSO_4 \cdot 0.5H_2O$. Figure 2e shows that blast furnace slag powder particles have uneven shapes, rough and uneven surfaces, and a particle size distribution mainly between 3 and 30 μm, good flowability, and a white color. The main chemical components are SiO_2 and Al_2O_3. Figure 2f shows that carbide slag particles vary greatly in shape, with rough surfaces and larger particles adhering to smaller ones. The particle size ranges from 10 to 100 μm, with good dispersion and a white color. The main chemical components are CaO and SiO_2. Overall, the materials are rich in active components like CaO, Al_2O_3, and SiO_2. These components can react synergistically in aqueous solutions to form stable C-(A)-S-H and AFt gels, providing a chemical foundation for preparing cementitious materials.

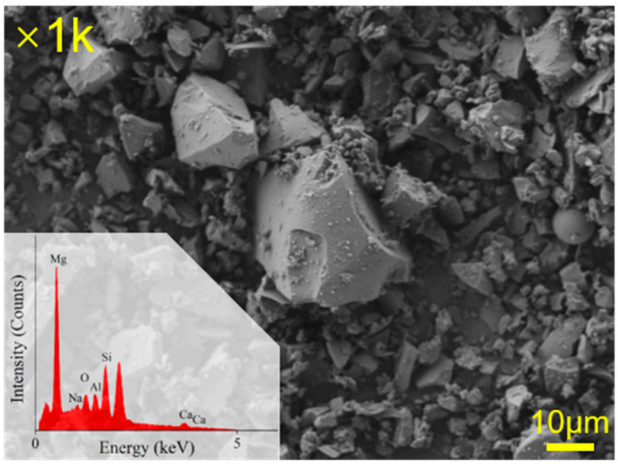

(**a**) CG

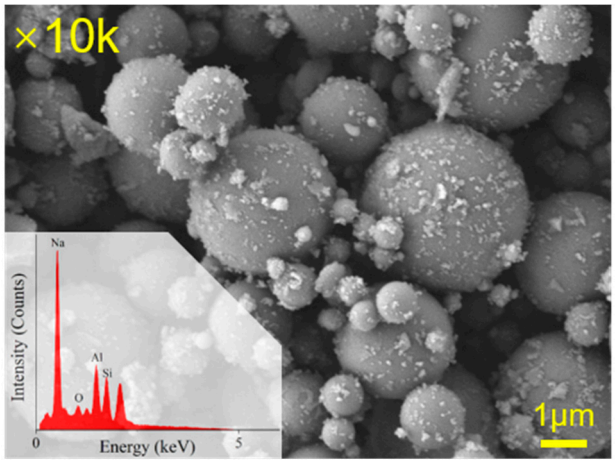

(**b**) FA

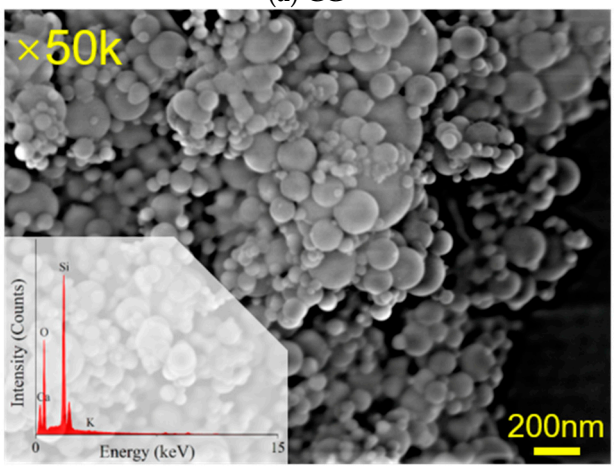

(**c**) SF

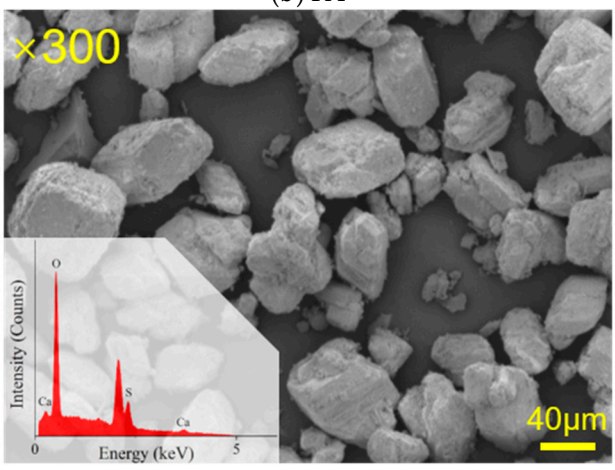

(**d**) DG

Figure 2. *Cont.*

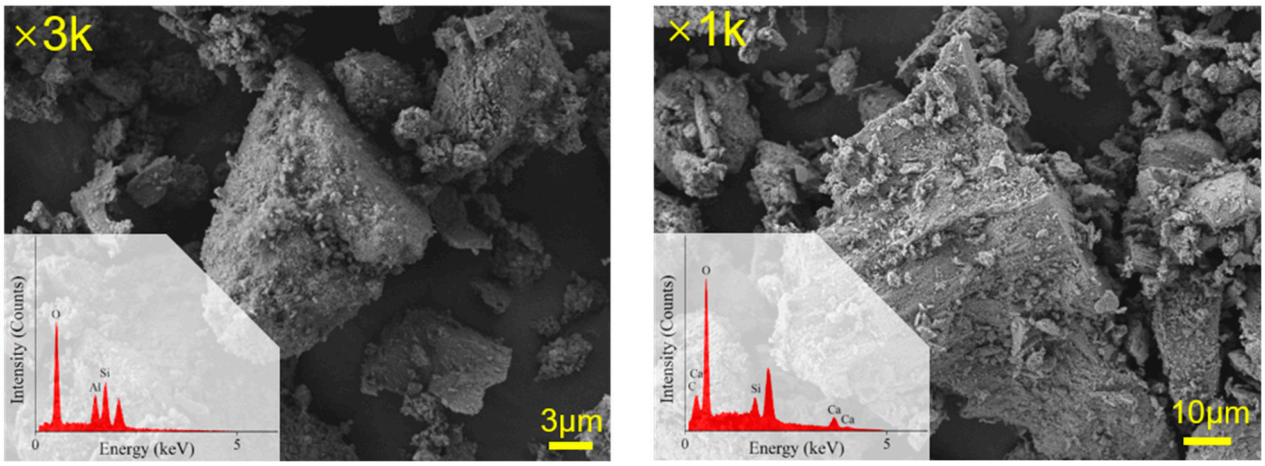

(**e**) BFS (**f**) CS

Figure 2. SEM and EDS of solid waste raw materials.

Table 2. The main chemical element content of solid waste raw materials.

Materials\Elements (Wt/%)	O	Si	Al	Ca	Na	Mg	S	K	C	Total
CG	37.29	19.16	5.64	32.03	1.31	4.57				100
FA	48.55	23.94	23.76		3.75					100
SF	47.38	22.76						0.22	29.64	100
DG	44.91			27.02			28.07			100
BFS	44.84	36.81	18.35							100
CS	33.06	5.65		58.29					3	100

2.2. Test Method

2.2.1. Contrast Test of Strength of Cemented RS and Stable AS

Given the large reserves of CG, nine different mix ratios were designed for comparison experiments based on activated coal gangue powder. As shown in Figure 3, the base materials were CG, FA, and DG. Gradually, the proportion of CG was reduced while adding SF, CS, and BFS.

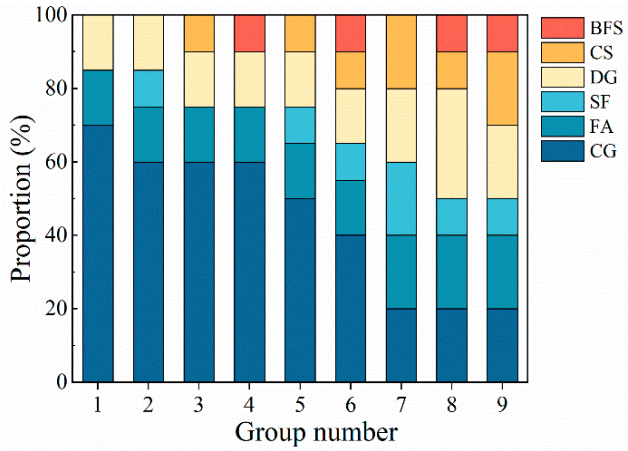

Figure 3. Comparative test material ratio combination design.

The sand's bending and compressive strength for industrial solid waste binders were tested in accordance with the specification [43] with a sand-to-binder ratio of 1:3 and a water-to-binder ratio of 1:2. The unconfined compressive strength of stabilized AS was

tested in accordance with the specification [44] with a total solid waste content of 30%, water content of 15%, and cylindrical specimens of φ 50 × h 50 mm weighing 205 ± 0.5 g.

The overall testing procedure is shown in Figure 4. First, the solid waste materials were dried, weighed according to the designed ratios, and then mixed and stirred for 3 min. The mixture was then combined with RS or AS, stirred for another 3 min, and water was added and mixed for 5 min. The AS samples were pre-moistened with half the water for 12 h. Next, the binder was poured into three-beam molds and vibrated for shaping, then demolded after 24 h. The AS samples were formed in cylindrical molds under static pressure for 2 h before demolding. The pressing speed was 1 mm/min. Finally, the samples were cured in a temperature and humidity-controlled chamber at 20 ± 2 °C and 95% humidity until the designated age, followed by strength testing and sampling. The loading speed of the compression test was 1 mm/min.

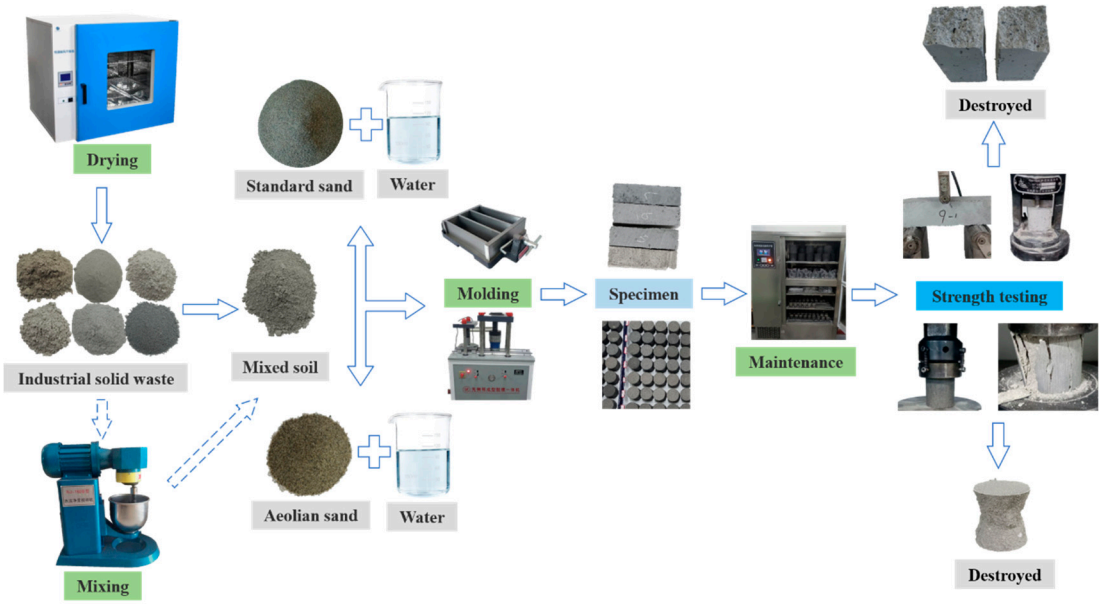

Figure 4. Solid waste cementitious material sample preparation and test flow chart.

2.2.2. Orthogonal Test

The orthogonal experiment design used 6 factors at 3 levels, as shown in Table 3. The levels were determined based on an initial evaluation of material reactivity from the first stage comparison tests and the chemical composition of the materials. Because CS has better activity performance in the comparative test, and the activity of CG is poor. And CS's high CaO content provides a conducive reaction environment, while DG's main component, $CaSO_4$, can react to form AFt. To ensure the strength of the solid waste combinations, we increased the proportion of more reactive materials and reduced that of less reactive ones. The levels for CS and DG were 2, 3, and 4, while FA, SF, and BFS were at levels 1, 2, and 3. The levels for CG were 0, 1, and 2.

Table 3. Orthogonal test designs table.

Material	Proportion of Dosage		
	Level I	**Level II**	**Level III**
CS	2	3	4
DG	2	3	4
FA	1	2	3
SF	1	2	3
BFS	1	2	3
CG	0	1	2

The AS mass ratio was set at 60%, with solid waste materials constituting 40% of the total mass. The ratios of solid waste materials followed the orthogonal design levels. For example, in the second orthogonal group, the material ratios were CS:DG:FA:SF:BFS:CG = 2:2:2:2:3:2, which translates to a total mass ratio of AS:CS:DG:FA:SF:BFS:CG = 60%:6.154%:6.154%:6.154%:6.154%:9.230%:6.154%. The results of the orthogonal experiment design are shown in Figure 5.

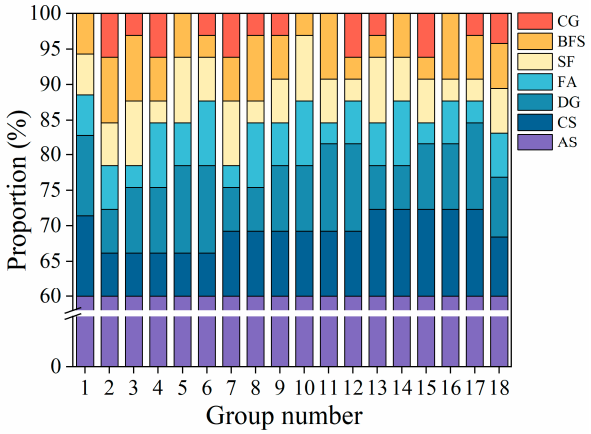

Figure 5. Orthogonal test ratio design results.

2.2.3. Strength Test of Solidified AS

Based on the optimal ratios from the orthogonal tests, strength testing of the stabilized AS was conducted. The final mix, detailed in Table 4, included CS at 28.56%, SF and BFS each at 21.43%, and DG and FA each at 14.29%.

SWCM was prepared in proportions of 10%, 20%, 30%, 40%, and 50% to stabilize AS, as shown in Figure 6. With increasing SWCM content, the surface color of the samples changed from yellow to white and then to black. Additionally, as the amount of AS decreased, the surface roughness of the samples also decreased. After standard curing for 3, 7, and 28 days, the samples were soaked in water on the last day, then dried and tested for unconfined compressive strength, as shown in Figure 7.

Table 4. The best ratio combination.

Materials	CS	DG	FA	SF	BFS
Proportion factor	4	2	2	3	3
Proportion (%)	28.56	14.29	14.29	21.43	21.43

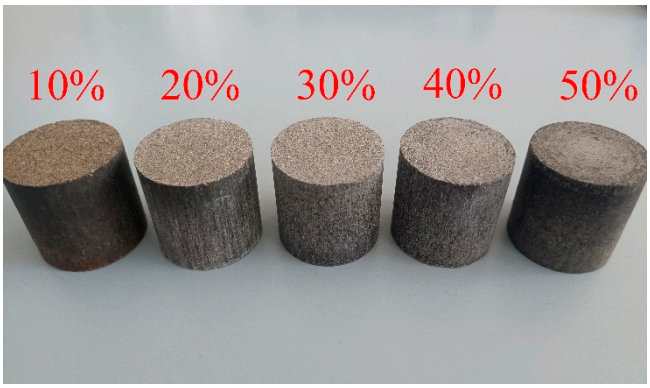

Figure 6. Different content of SWCM solidified AS test block.

Figure 7. Unconfined compressive strength test.

2.2.4. Microscopic Test Methods

The molecular structure and chemical composition of SWCM-stabilized AS were analyzed using the Bruker INVENIO Fourier-transform infrared spectrometer (Bruker, Billerica, MA, USA) to identify the types of chemical products and compare compositional changes. Bruker D8 Advance X-ray Powder Diffraction was used to obtain diffraction peaks and angles for different SWCM-stabilized AS samples, analyzing their compositional forms and reactivity characteristics. The JSM-IT800 Field Emission Scanning Electron Microscope (JEOL Ltd., Akishima, Japan) observed the microstructure of the samples with varying SWCM content and ages, analyzing surface features. Additionally, the integrated JEOL X-ray Energy Dispersive Spectrometer (EDS) was used for rapid elemental analysis of microregions to identify chemical products and components.

3. Results and Discussion

3.1. Comparative Test Result

The strength test results for binder-stabilized RS are shown in Figure 8. Strength increases with age across all mix ratios, with similar patterns for bending and compressive strengths. Figure 8a shows that bending strengths for groups 1, 2, and 3 is below 0.2 MPa at all ages, and Figure 8b shows compressive strengths below 0.4 MPa. This indicates low activity in the solid waste binder system when using CG as the main component, or that the activity was not activated with this mix. In contrast, group 4, with added CS, showed significant strength improvement, with average bending and compressive strengths increasing by 9.5 and 16.4 times, respectively. Groups 5 to 9, which included CS and reduced CG, also saw varying degrees of strength improvement. In particular, group 7 achieved maximum mechanical strength with 20% CS, reaching 2.7 MPa for bending strength and 11.7 MPa for compressive strength at 28 days. This indicates a strong activity of the CS. In the mix of six solid waste materials, carbide slag's high CaO content generates $Ca(OH)_2$, providing an alkaline environment that activates further chemical reactions to form C-S-H, C-A-S-H, and AFt gels, enhancing mechanical strength [45]. Additionally, the strength growth rate from 3 to 7 days was significantly higher than from 7 to 28 days, indicating a gradual decrease in hydration reaction over time.

Comparing the material ratios and strength results of groups 1 to 4, it is evident that CS contributes more to strength than SF, DG, FA, CG, and BFS. Comparisons of groups 5 and 6 show that reducing CG and adding BFS increased strength, indicating BFS has a greater strength contribution than CG. Comparisons between groups 2 and 3, and 7 and 9 show that adding BFS and reducing SF decreased strength, suggesting BFS's strength contribution is lower than SF's in this mix. Therefore, the preliminary strength contribution ranking of materials is: CS > SF > BFS > CG, providing a basis for further orthogonal test design.

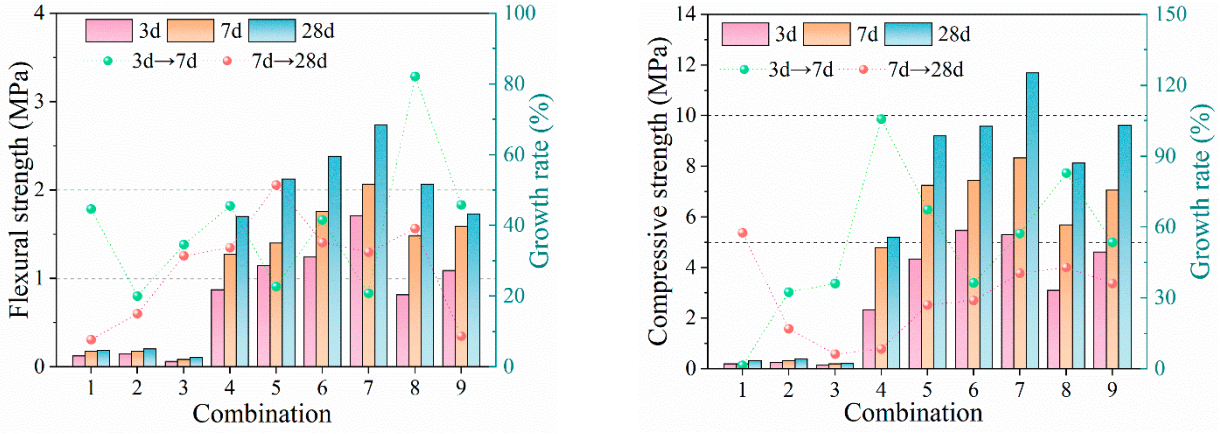

(**a**) Bending strength results (**b**) Compressive strength results

Figure 8. Strength test results of solid waste cemented RS.

The UCS results for stabilized AS are shown in Figure 9. As seen in Figure 9a, strength increases with curing time for all mix ratios. Groups 1, 2, and 3 have strengths below 0.5 MPa, indicating that the solid waste materials did not effectively bind the AS. Groups 4 to 9, with strengths nearing or exceeding 3 MPa at 7 days, show significant strength increase with the addition of CS. Compared to binder-stabilized RS, the strength of binder-stabilized AS increases slowly from 3 to 7 days. Figure 9b shows a significant decrease in strength after immersion; strengths for groups 1 to 3 approach 0 MPa, indicating poor water stability. In contrast, groups 4 to 9 (excluding group 7) have water stability coefficients between 20% and 40%, with group 7 showing a significant increase in water stability due to a higher CS content.

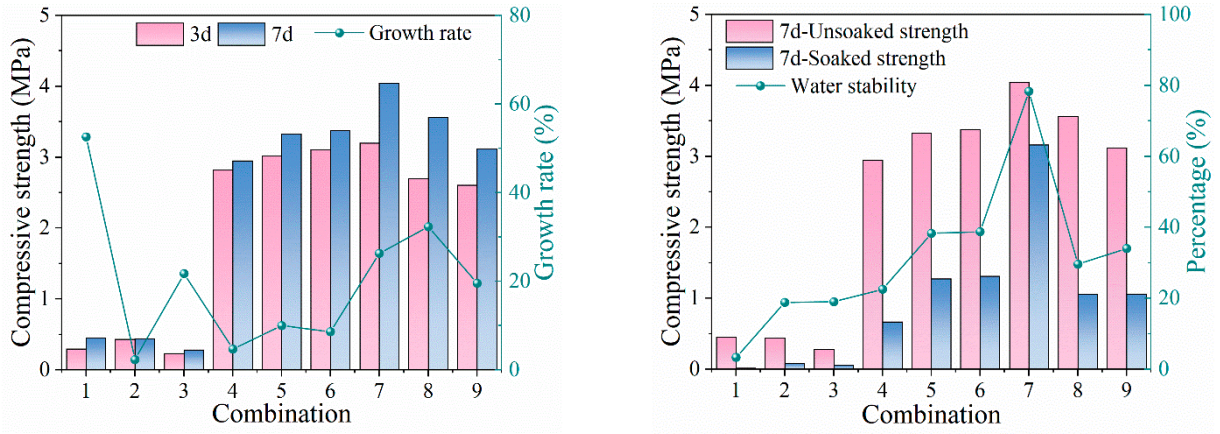

(**a**) Compressive strength (**b**) Water stability test results

Figure 9. Strength test results of solid waste stabilized AS.

The analysis indicates that various solid wastes can effectively bind RS when used in appropriate ratios, demonstrating the feasibility of creating a binder material fully from solid waste. AS, being a special construction material with poor gradation characteristics, shows slow strength growth and inadequate water stability when stabilized with solid waste. Additionally, minimal synergistic reactivity was observed among CG, FA, SF, DG, and BFS, while the addition of CS provides an alkaline environment, enhancing strength through pozzolanic reactions. Comparing the compressive strengths of binder-stabilized RS and stabilized AS, the former shows a greater increase in strength with age, while the latter's strength growth is modest. Binder-stabilized RS exhibits 1 to 2.5 times higher strength than AS, despite only a 3.33% increase in binder content, primarily due to the

larger particle size of RS, suggesting that increasing the particle size of stabilizing materials can improve mechanical strength.

3.2. Orthogonal Test Results

3.2.1. Average Strength Values

The average strength values from orthogonal tests for each solid waste material at different ratios and ages are shown in Figure 10. It is observed that the strength of all six solid wastes increases with age for each mix ratio, but there is a notable decrease in strength after immersion. The average ratio of 7-day strength after immersion to the 7-day strength without immersion is about 50%, indicating that the water stability of AS stabilized with these six material combinations is relatively low.

From Figure 10a,d,e, it can be seen that the 7-day strength of CS, SF, and BFS increases with higher mix ratios. Figure 10c shows that the 7-day strength of FA increases and then decreases with higher mix ratios. Figure 10b,f reveal that the 7-day strength of DG and CG decreases with increasing mix ratios. SF achieves its maximum UCS-7d strength of 8.99 MPa at the K3 level, while the minimum strength of 6.75 MPa is observed at the K1 level for CS. This indicates that SF and CS have a significant impact on strength, with higher SF providing greater strength and lower CS lacking a reactive environment, thus failing to achieve adequate strength. Comparing the UCS-7d strength change rates, SF and CS show more significant strength changes with varying mix ratios, while BFS and CG have a smaller impact on strength.

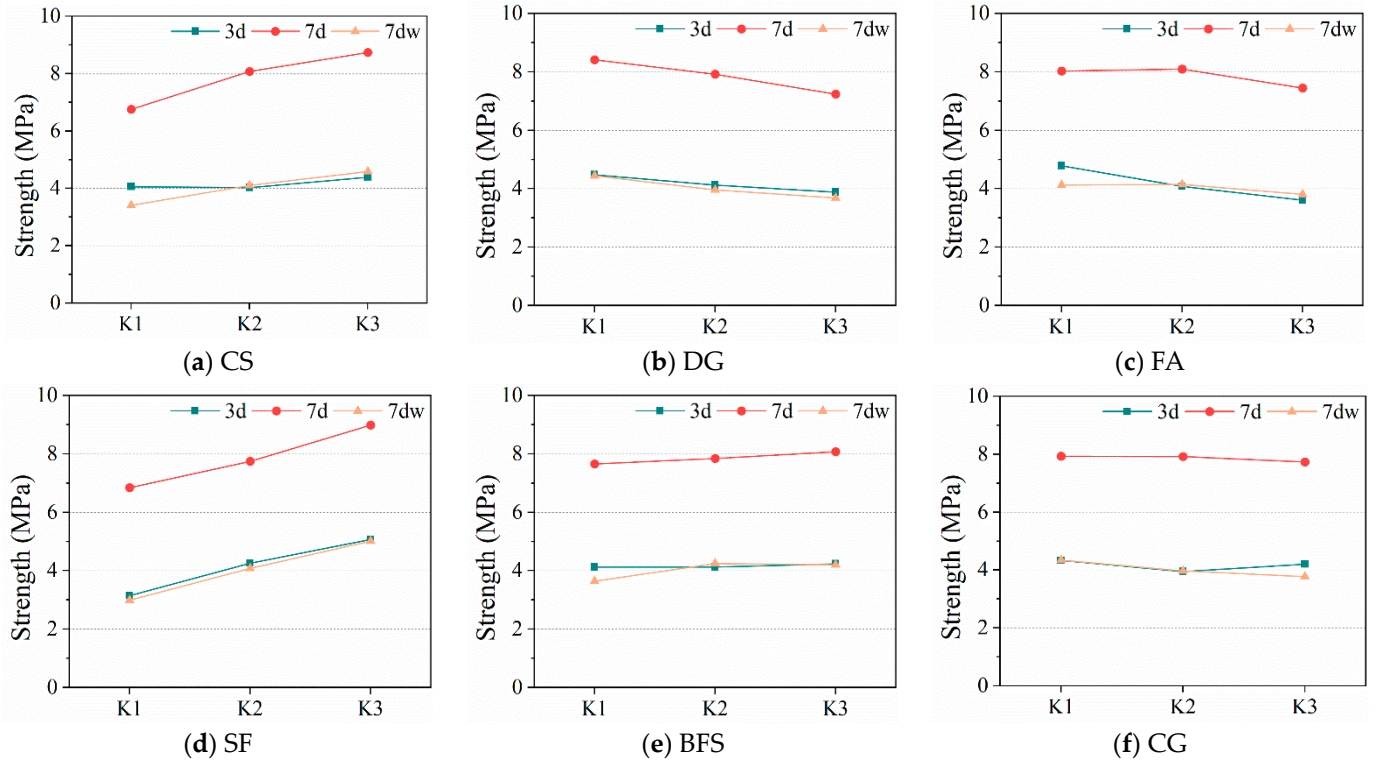

Figure 10. The variation law of mean intensity.

3.2.2. Range Analysis Results

The range analysis results are shown in Table 5. The strength contribution rates, in descending order, are SF, CS, DG, FA, BFS, and CG. The strength variation for each solid waste material at different mix ratios is illustrated in Figure 11, revealing that the optimal mix ratio is $A_3B_1C_2D_3E_3F_1$.

Table 5. Range calculation results.

Group	Compressive Strength					
	A (CS)	B (DG)	C (FA)	D (SF)	E (BFS)	F (CG)
k1	3.41	4.44	4.13	2.99	3.64	4.35
k2	4.10	3.96	4.15	4.08	4.25	3.97
k3	4.59	3.69	3.81	5.02	4.20	3.77
R	1.18	0.75	0.34	2.03	0.61	0.58
Effect sequence	SF > CS > DG > FA > BFS > CG					
Optimal Composition	$A_3B_1C_2D_3E_3F_1$					

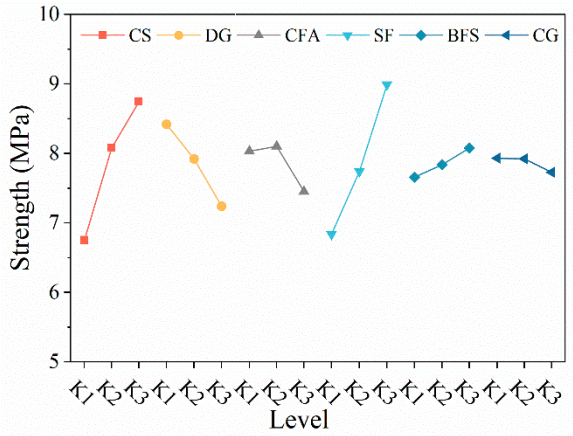

Figure 11. Comparison of mean strength change rules.

3.2.3. Variance Analysis

The variance analysis results are shown in Table 6. The analysis indicates that CS and SF have a particularly significant impact on overall strength, while DG has a significant effect, and FA, BFS, and CG do not have significant impacts. The order of impact is SF > CS > DG > FA > BFS > CG, which is consistent with the range analysis results. However, unlike the comparative test results, orthogonal testing reveals that changes in SF levels cause more significant strength variations compared to CS. This is because CS provides a chemical reaction base, while SF, due to its low density, has a physical filling effect and high SF content results in a higher initial density.

Table 6. Variance calculation results.

Source	Square Deviation	Freedom	F	Significance
CS	12.338	2	26.05	0.002
DG	4.192	2	8.851	0.023
FA	1.54	2	3.252	0.125
SF	14.035	2	29.633	0.002
BFS	0.518	2	1.093	0.404
CG	0.163	2	0.344	0.725
Error	1.184	5		

3.2.4. Linear Regression

By using the solid waste content factors as independent variables, a linear regression equation relating content factors to strength can be derived, as shown in Equation (1), with $R^2 = 0.93$. The fitted and predicted results are illustrated in Figure 12. Based on the orthogonal test mean analysis, range analysis, and variance analysis, the optimal mix ratio for the solid waste materials is shown in Figure 13, with CS at 28.57%, SF and BFS each at 21.43%, and DG and FA each at 14.29%.

$$Y = 0.995X_1 - 0.58833X_2 - 0.28833X_3 + 1.07667X_4 + 0.20667X_5 - 0.10167X_6 + 4.75111 \quad (1)$$

where: X_1 is CS, X_2 is DG, X_3 is FA, X_4 is SF, X_5 is BFS, and X_6 is CG.

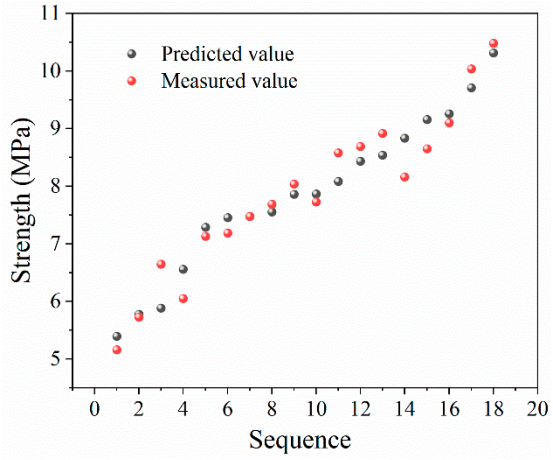

Figure 12. Comparison of Linear Regression Results.

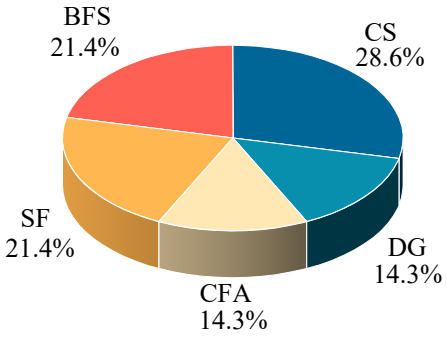

Figure 13. The best proportion of materials.

3.3. Strength Test Result of Solidified AS

Figure 14 shows the relationship between SWCM content and the strength of stabilized AS. From Figure 14a, it is evident that the strength has a strong linear correlation with SWCM content across different ages. Table 7 shows that the correlation coefficient (R^2) is greater than 0.98. The parameter *k* represents the rate of strength increase, which increases as the SWCM content rises. This indicates that with more SWCM, the quantity of hydration gels produced from chemical reactions increases, thereby accelerating the rate and extent of strength gain. Additionally, Figure 6 shows that, as the SWCM proportion increases, gradation improves and surface roughness decreases, indicating that SWCM also contributes to physical improvements. Figure 14b depicts how strength varies with age and SWCM content. The UCS strength consistently increases with age. According to Figure 15, the average strength growth rate from 3 to 7 days is significantly higher than that from 7 to 28 days, except when the SWCM content is 10%. As SWCM content increases, the average strength growth rate from 3 to 7 days shows a trend of initially increasing, then decreasing, and finally increasing again, while the rate from 7 to 28 days continually decreases. This indicates that as curing age extends, the reactive components in the waste are gradually depleted, reducing the volume of hydration reactions and thus slowing the rate of strength gain.

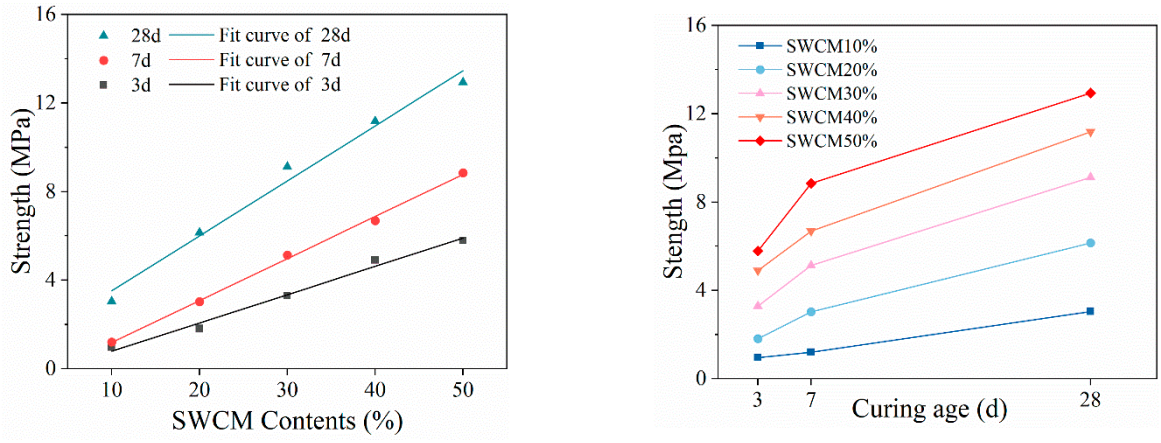

(**a**) Different SWCM content (**b**) Different ages

Figure 14. Mechanical strength characteristics of SWCM solidified AS.

Table 7. The linear fitting parameters of the relationship between SWCM content and strength at different ages.

Curing Age (d)	Relational Expression	*k*	a	Residual Sum of Squares	R^2
3 d	$y = kx + a$	0.1276	−0.4774	0.1890	0.9885
7 d	$y = kx + a$	0.1895	−0.7055	0.0706	0.9980
28 d	$y = kx + a$	0.2483	1.0387	0.9533	0.9848

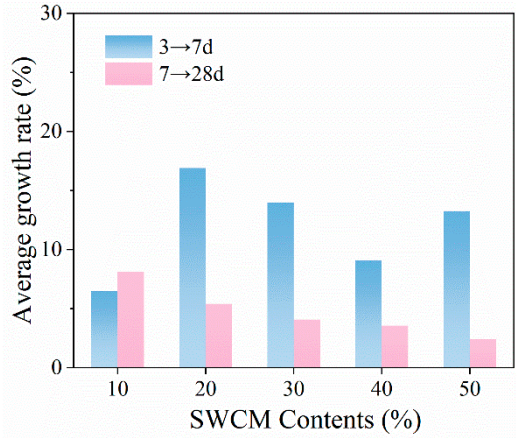

Figure 15. Different curing age and strength growth rate.

Figure 16 shows the water stability test results for SWCM-stabilized AS. It is observed that the strength decreases after immersion under various ages and mix ratios. Specifically, at 7 days, a higher SWCM content leads to greater strength loss upon immersion and decreased water stability. At 28 days, the water stability coefficient fluctuates between 75% and 86%. When the SWCM content reaches or exceeds 30%, there is a noticeable decline in the water stability coefficient. The effectiveness of completely industrial waste-based binders is limited due to the restricted content of active components and resultant chemical reactions. This limitation prevents full curing of wind-blown sand. Additionally, finer particle sizes of solid waste materials increase the micro-porosity of samples. Through the SEM test, it can be seen that increased SWCM content leads to more micro-cracks due to hydration shrinkage. These pores and cracks provide pathways for water infiltration, weakening the inter-particle bonding and reducing frictional resistance. Under load, capillary water pressure forms inside the material, further decreasing its water stability.

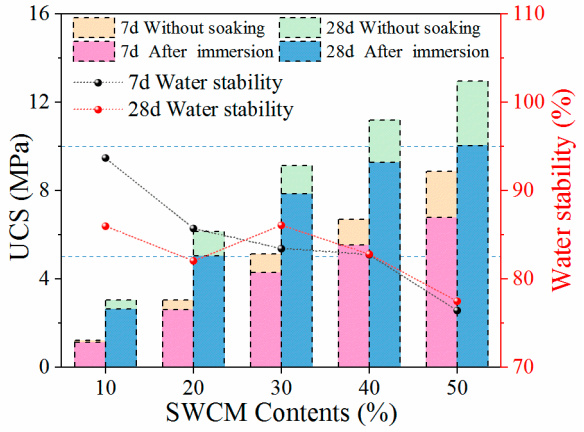

Figure 16. Different UCS strength and water stability.

According to the specification [46], the UCS standard for industrial waste-based stabilizing materials should exceed 1.1 MPa for subbase applications. This study shows that when SWCM content reaches 20% or more, the strength of the stabilized AS meets the regulatory requirements. By adjusting the SWCM content, the material can be suitable for subbase construction in various road classes.

3.4. Microstructural Properties

3.4.1. FTIR Analysis

Figure 17 shows the infrared spectra of stabilized AS with different SWCM contents after 28 days. It is observed that with increasing SWCM content, the O-H bond peak from $Ca(OH)_2$ at 3643 cm^{-1} becomes more pronounced. Peaks for crystalline water's -OH bonds at 3448 cm^{-1} and 1624 cm^{-1}, carbonate C-O bonds at 1426 cm^{-1}, Si-O bonds in C-(A)-S-H at 1148 cm^{-1}, 1007 cm^{-1}, and 455 cm^{-1}, and Al-O bonds in ettringite and C-A-S-H gel at 874 cm^{-1} also increase [45,47,48]. This indicates that higher SWCM content promotes the formation of silicoaluminate gels and carbonates in the hydration products.

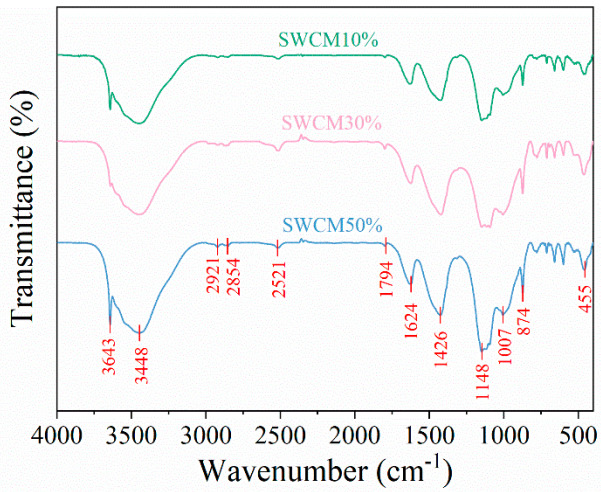

(**a**) FTIR spectra 400~4000.

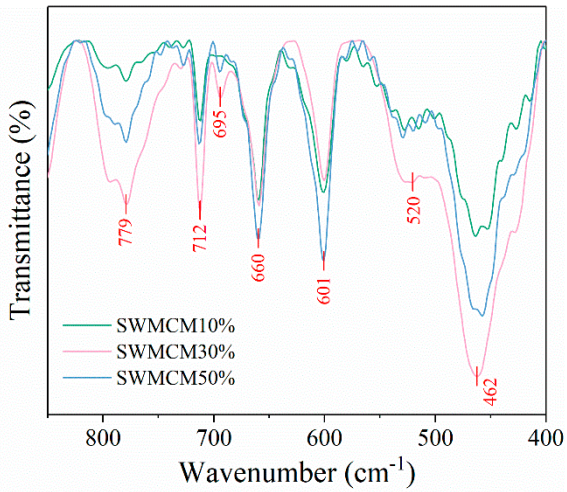

(**b**) FTIR spectra 400~900.

Figure 17. FTIR test results of 28 d with different SWCM contents.

Figure 17b shows that at peaks of 779 cm^{-1}, 712 cm^{-1}, 520 cm^{-1}, and 462 cm^{-1}, the intensity for SWCM30% exceeds that of SWCM50%, while at 660 cm^{-1} and 601 cm^{-1}, SWCM50% shows the highest intensity. The intensity of peaks related to residual materials like SiO_2 decreases with increasing SWCM content. Additionally, higher SWCM content shifts the peaks towards higher frequencies, likely due to structural changes within the

molecules or interactions with metal ions in the materials, forming solid solutions with the gel [49].

3.4.2. SEM Analysis

Figure 18 illustrates the microstructural characteristics of SWCM-stabilized AS with 10%, 30%, and 50% SWCM content after 28 days of curing. Figure 18a shows that the sand particles are coated with an amorphous hydration gel, though the gel coverage is limited. Visible cracks and small pores are present due to dehydration and shrinkage, formed by particle voids and material dissolution. Figure 18b,c reveal that as SWCM content increases, the gel coverage significantly expands. At 30% SWCM, the surface gel appears as a network of amorphous composite gel. At 50% SWCM, distinct rod-like gels appear and interweave. With continued hydration, these rod-like gels grow into plate-like and amorphous colloids. Figure 18c also shows partially reacted FA particles with needle-like gels on their surface, connected to the bottom cluster gels.

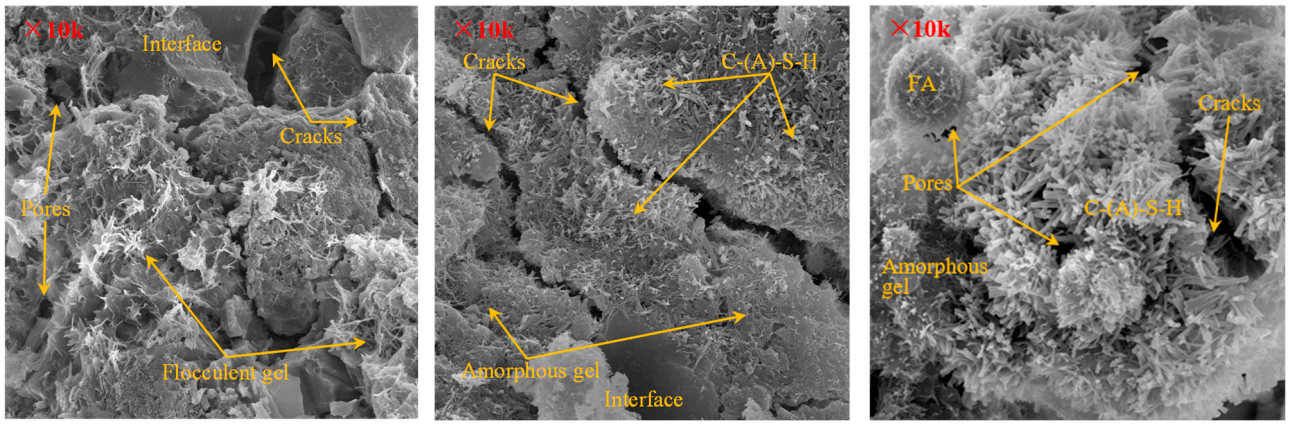

(**a**) SWCM10% (**b**) SWCM30% (**c**) SWCM50%

Figure 18. SEM images of different contents of SWMCM solidified AS.

Figure 19a shows that the rod-like gel at point 'a' in Figure 19d mainly consists of Ca, O, and Si, indicating that its chemical composition is C-S-H. Figure 19b,c reveal the presence of carbon, suggesting that the amorphous region contains a mix of carbonate and silicate gels. Carbonates are primarily formed by the reaction of CaO from carbide slag with water to produce $Ca(OH)_2$, which then reacts with CO_2 to form calcium carbonate precipitation.

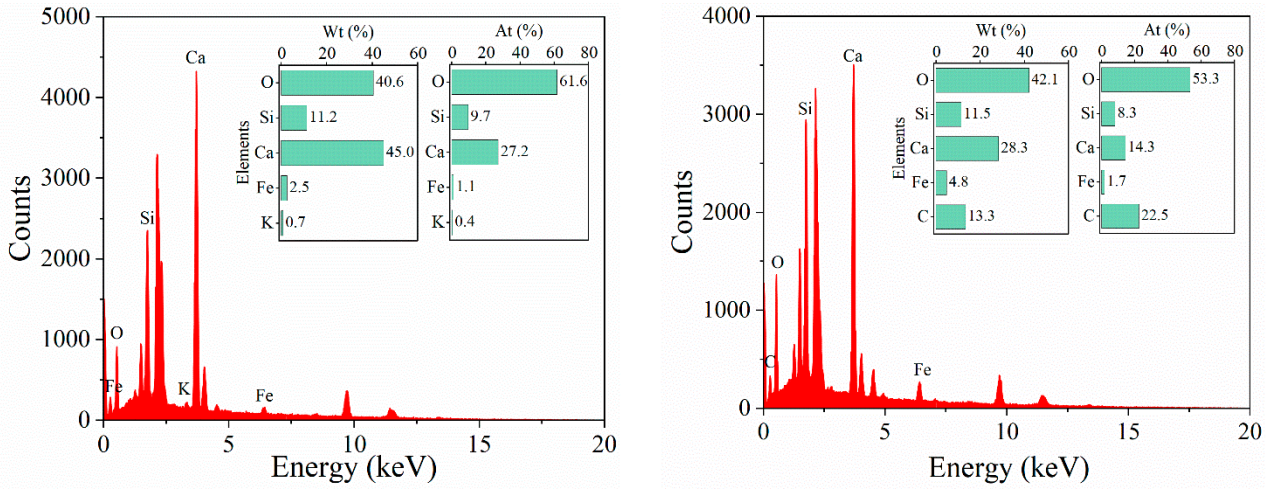

(**a**) Spot-a. (**b**) Spot-b.

Figure 19. *Cont.*

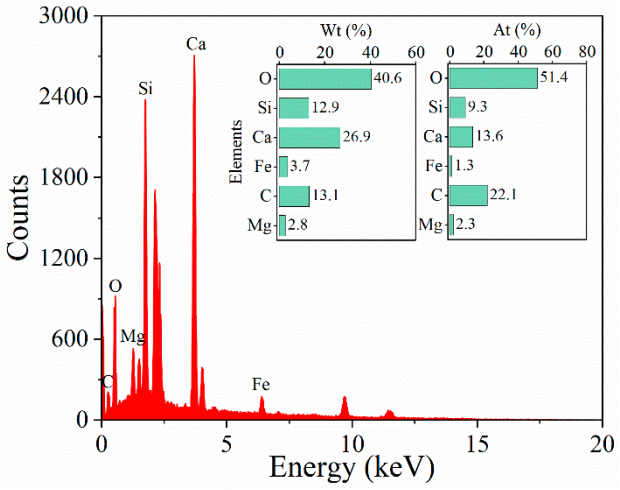

(**c**) Spot-c.

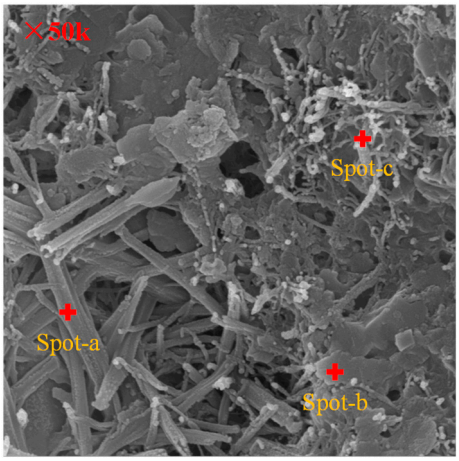

(**d**) EDS test point diagram.

Figure 19. EDS spectrum.

3.4.3. XRD Analysis

Figure 20 shows the XRD diffraction patterns of stabilized AS with different SWCM contents after 28 days. The most prominent peaks are for SiO_2, followed by $CaCO_3$. The peaks for hydrated silicate gel are weaker due to its complex structure and the presence of AFt and $Ca(OH)_2$. Additionally, partially unreacted $CaSO_4 \cdot 0.5H_2O$ crystals are detected around $2\theta = 14.7°$. As SWCM content increases, peaks for SiO_2 and $CaSO_4 \cdot 0.5H_2O$ diminish and eventually disappear, indicating more complete chemical reactions and near-total consumption of raw materials at higher SWCM levels. The XRD results show that the main hydration products are calcium silicate hydrate, calcium aluminate hydrate, calcium carbonate, and ettringite. Key chemical reactions include CaO from carbide slag reacting with water to produce OH^- ions. In an alkaline environment, materials dissolve, releasing acid anions and metal cations. As shown in Formulas (2)–(9). SiO_2 and Al_2O_3 dissolve to form $[H_3SiO_4]^-$ and $[H_3AlO_4]^{2-}$, which further form $[Al(OH)_6]^{3-}$. $CaSO_4 \cdot 0.5H_2O$ provides Ca^{2+} and SO_4^{2-}; $[Al(OH)_6]^{3-}$ ions combine with Ca^{2+} and SO_4^{2-} to form AFt; $[H_3SiO_4]^-$ with Ca^{2+} and H_2O generates C-S-H; $[H_3SiO_4]^-$ and $[H_3AlO_4]^{2-}$ with Ca^{2+} form C-A-S-H; and $Ca(OH)_2$ reacts with CO_2 in the air to produce $CaCO_3$ [45,50].

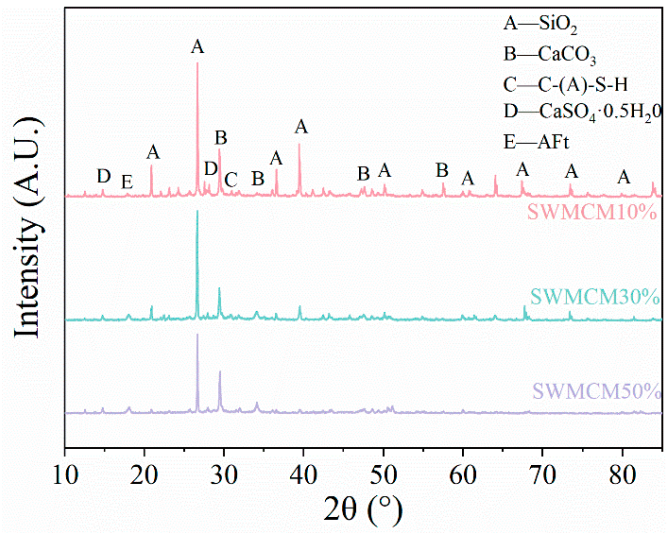

Figure 20. XRD test results of 28 d with different SWCM content.

Therefore, it can be seen that the key component, CaO, plays a crucial role in the strength of the system. CaO provides activation and hydration effects; a sufficient amount is needed to activate other potentially reactive components and promote their hydration reactions [51,52]. As the proportion of SWCM increases, the formation of hydration gels like calcium silicate and calcium aluminate increases, enhancing the material's strength.

$$SiO_2 + OH^- + H_2O \rightarrow [H_3SiO_4]^- \quad (2)$$

$$Al_2O_3 + OH^- \rightarrow AlO_2{}^- + H_2O \quad (3)$$

$$AlO_2{}^- + OH^- + H_2O \rightarrow [H_3AlO_4]^{2-} \quad (4)$$

$$[H_3AlO_4]^{2-} + OH^- + H_2O \rightarrow [Al(OH)_6]^{3-} \quad (5)$$

$$[Al(OH)_6]^{3-} + Ca^{2+} + SO_4^{2-} + H_2O \rightarrow Ca_6Al_2(SO_4)_3(OH)_{12}{\cdot}26H_2O \quad (6)$$

$$[H_3SiO_4]^- + [H_3AlO_4]^{2-} + Ca^{2+} \rightarrow mCaO \cdot nSiO_2 \cdot pAl_2O_3 \cdot qH_2O \quad (7)$$

$$[H_3SiO_4]^- + Ca^{(2+)} + H_2O \rightarrow Ca_xSiO_{2+x} \cdot nH_2O \quad (8)$$

$$Ca^{2+} + OH^- + CO_2 \rightarrow CaCO_3 + H_2O \quad (9)$$

4. Conclusions

(1) Carbide slag provides an alkaline environment that promotes hydration reactions, thereby increasing the strength of waste-based cementitious materials. Compared to stabilized AS, the strength of stabilized RS is higher, indicating that increasing the main material's particle size effectively enhances strength.

(2) Orthogonal test analysis shows that the sensitivity of strength for waste-stabilized AS is in the order of SF > CS > DG > FA > BFS > CG. The optimal mix ratio is CS:DG:FA:SF:BFS = 4:2:2:3:3.

(3) The SWCM content is linearly related to the strength of stabilized AS. Initially, strength increases more rapidly with higher SWCM content, but later exhibits the opposite trend. Overall water stability decreases with increasing SWCM content. Adjusting SWCM content can make stabilized AS meet the requirements for various road base levels.

(4) With lower SWCM content, hydration reactions are insufficient, and the active components in the waste do not fully react. As SWCM content increases, the quantity of hydration products increases. The main hydration products of SWCM-stabilized AS are calcium silicate hydrate, calcium aluminate hydrate, calcium carbonate, and ettringite.

Research on SWCM cementitious materials provides a reference for waste utilization and green building materials. Future studies could further optimize the mix ratios of all-waste cementitious materials and comprehensively study the mechanical properties of stabilized AS to advance waste utilization and desert road construction.

Author Contributions: Conceptualization, J.C.; methodology, Y.D.; validation, A.M.; formal analysis and investigation, Z.P.; resources, J.C.; data curation, Y.D.; writing—original draft preparation, A.M.; writing—review & editing and supervision, Y.W. All authors have read and agreed to the published version of the manuscript.

Funding: This research was funded by Study on the Application Performance of Aeolian Sand Improved by Ternary Solid Waste Cementitious Material, grant number KSGSGCJS-24-ZXFWHT-004.

Data Availability Statement: The original contributions presented in the study are included in the article, further inquiries can be directed to the corresponding author.

Conflicts of Interest: Author Akelamjiang Maimait was employed by the company Xinjiang Kusha Highway Development Limited Liability Company. The remaining authors declare that the research was conducted in the absence of any commercial or financial relationships that could be construed as a potential conflict of interest.

References

1. Feng, L.; Yao, W.; Zheng, K.; Cui, N.; Xie, N. Synergistically Using Bauxite Residue (Red Mud) and Other Solid Wastes to Manufacture Eco-Friendly Cementitious Materials. *Buildings* **2022**, *12*, 117. [CrossRef]
2. Garanayak, L. Strength effect of alkali activated red mud slag cement in ambient condition. *Mater. Today Proc.* **2021**, *44*, 1437–1443. [CrossRef]
3. Zhu, J.; Yue, H.; Ma, L.; Li, Z.; Bai, R. The synergistic hydration mechanism and environmental safety of multiple solid wastes in red mud-based cementitious materials. *Environ. Sci. Pollut. Res.* **2023**, *30*, 79241–79257. [CrossRef] [PubMed]
4. Ren, C.; Wang, W.; Hua, D.; Wu, S.; Yao, Y. Preparation and Properties of a Sulphoaluminate Magnesium-Potassium Phosphate Green Cementitious Composite Material from Industrial Solid Wastes. *Materials* **2021**, *14*, 7340. [CrossRef]
5. Zhang, Y.; Wang, J.; Zhang, L.; Li, C.; Jiang, H.; Ba, X.; Hou, D. Study on the preparation and properties of high-belite cementitious materials from shield slag and calcium carbide slag. *Constr. Build. Mater.* **2022**, *355*, 129082. [CrossRef]
6. Carvalho, V.R.; Costa, L.C.B.; Elói, F.P.d.F.; Bezerra, A.C.d.S.; de Carvalho, J.M.F.; Peixoto, R.A.F. Performance of low-energy steel slag powders as supplementary cementitious materials. *Constr. Build. Mater.* **2023**, *392*, 131888. [CrossRef]
7. Wang, Y.H.; Cai, J.; Ding, P.P. Investigation on High Volume Steel Slag—Rice Husk Ash Composite Binder Properties. *Key Eng. Mater.* **2014**, *599*, 310–314. [CrossRef]
8. Filazi, A.; Demir, I.; Sevim, O. Enhancement on mechanical and durability performances of binary cementitious systems by optimizing particle size distribution of fly ash. *Arch. Civ. Mech. Eng.* **2020**, *20*, 58. [CrossRef]
9. Li, X.; Ma, X.; Zhang, S.; Zheng, E. Mechanical Properties and Microstructure of Class C Fly Ash-Based Geopolymer Paste and Mortar. *Materials* **2013**, *6*, 1485–1495. [CrossRef]
10. Demir, I.; Filazi, A.; Sevim, O.; Simsek, O. Influence of freeze–thaw cycling on properties of cementitious systems doped with fly ash having optimized particle size distribution. *Arch. Civ. Mech. Eng.* **2022**, *22*, 189. [CrossRef]
11. Wang, K.; Fu, J.-X.; Wang, J. The ratio optimization and hydration mechanism of multi source solid waste cementitious materials. *Constr. Build. Mater.* **2024**, *411*, 134267. [CrossRef]
12. Yang, P.; Liu, L.; Suo, Y.; Qu, H.; Xie, G.; Zhang, C.; Deng, S.; Lv, Y. Investigating the synergistic effects of magnesia-coal slag based solid waste cementitious materials and its basic characteristics as a backfill material. *Sci. Total Environ.* **2023**, *880*, 163209. [CrossRef]
13. Liu, J.; Song, G.; Ge, X.; Liu, B.; Liu, K.; Tian, Y.; Wang, X.; Hu, Z. Experimental Study on the Properties and Hydration Mechanism of Gypsum-Based Composite Cementitious Materials. *Buildings* **2024**, *14*, 314. [CrossRef]
14. Wang, Y.; Liu, X.; Zhu, X.; Zhu, W.; Yue, J. Synergistic effect of red mud, desulfurized gypsum and fly ash in cementitious materials: Mechanical performances and microstructure. *Constr. Build. Mater.* **2023**, *404*, 133302. [CrossRef]
15. Wu, P.; Zeng, Q.; Liu, X.; Zhang, Z.; Wei, C.; Li, Y.; Ma, S. Synergistic preparation of high-performance composite blast furnace slag powder from multiple industrial solid wastes: Performance regulation and optimization. *Constr. Build. Mater.* **2024**, *411*, 134231. [CrossRef]
16. Tang, C.; Mu, X.; Ni, W.; Xu, D.; Li, K. Study on Effects of Refining Slag on Properties and Hydration of Cemented Solid Waste-Based Backfill. *Materials* **2022**, *15*, 8338. [CrossRef]
17. Wu, X.; Li, B.; Wei, D.; Guo, F.; Ji, H. Investigation of Preparation and Shrinkage Characteristics of Multi-Source Solid Waste-Based Cementitious Materials. *Materials* **2023**, *16*, 7522. [CrossRef]
18. Gu, K.; Chen, B.; Pan, Y. Utilization of untreated-phosphogypsum as filling and binding material in preparing grouting materials. *Constr. Build. Mater.* **2020**, *265*, 120749. [CrossRef]
19. Xue, F.; Wang, T.; Zhou, M.; Hou, H. Self-solidification/stabilisation of electrolytic manganese residue: Mechanistic insights. *Constr. Build. Mater.* **2020**, *255*, 118971. [CrossRef]
20. Zhao, Y.; Qiu, J.; Ma, Z.; Sun, X. Eco-friendly treatment of coal gangue for its utilization as supplementary cementitious materials. *J. Clean. Prod.* **2021**, *285*, 124834. [CrossRef]
21. Guo, Y.; Yan, K.; Cui, L.; Cheng, F. Improved extraction of alumina from coal gangue by surface mechanically grinding modification. *Powder Technol.* **2016**, *302*, 33–41. [CrossRef]
22. Jiang, G.; Wu, A.; Wang, Y.; Lan, W. Low cost and high efficiency utilization of hemihydrate phosphogypsum: Used as binder to prepare filling material. *Constr. Build. Mater.* **2018**, *167*, 263–270. [CrossRef]
23. Gu, K.; Chen, B. Loess stabilization using cement, waste phosphogypsum, fly ash and quicklime for self-compacting rammed earth construction. *Constr. Build. Mater.* **2020**, *231*, 117195. [CrossRef]
24. Wu, H.; Xu, J.; Yang, D.; Ma, Z. Utilizing thermal activation treatment to improve the properties of waste cementitious powder and its newmade cementitious materials. *J. Clean. Prod.* **2021**, *322*, 129074. [CrossRef]
25. Shi, R.; Li, Y.; Mi, Q.; Zou, C.; Li, B. Thermodynamic Study on the Direct Reduction of Specularite by Lignite and the Coupling Process for the Preparation of Cementitious Material. *Minerals* **2022**, *12*, 354. [CrossRef]
26. Shi, R.; Li, X.; Cui, Y.; Zhao, J.; Zou, C.; Qiu, G. Coupled Preparation of Ferronickel and Cementitious Material from Laterite Nickel Ores. *Materials* **2020**, *13*, 4992. [CrossRef]
27. Zhao, P.; Jing, M.; Feng, L.; Min, B. The heavy metal leaching property and cementitious material preparation by treating municipal solid waste incineration fly ash through the molten salt process. *Waste Manag. Res.* **2020**, *38*, 27–34. [CrossRef]
28. Mao, Y.; Wu, H.; Wang, W.; Jia, M.; Che, X. Pretreatment of municipal solid waste incineration fly ash and preparation of solid waste source sulphoaluminate cementitious material. *J. Hazard. Mater.* **2020**, *385*, 121580. [CrossRef]

29. Su, C.; Zhang, J.; Ding, Y. Research on reactivity evaluation and micro-mechanism of various solid waste powders for alkali-activated cementitious materials. *Constr. Build. Mater.* **2024**, *411*, 134374. [CrossRef]
30. Alam, S.; Das, S.K.; Rao, B.H. Strength and durability characteristic of alkali activated GGBS stabilized red mud as geo-material. *Constr. Build. Mater.* **2019**, *211*, 932–942. [CrossRef]
31. Burciaga-Díaz, O.; Betancourt-Castillo, I. Characterization of novel blast-furnace slag cement pastes and mortars activated with a reactive mixture of MgO-NaOH. *Cem. Concr. Res.* **2018**, *105*, 54–63. [CrossRef]
32. Puertas, F.; Torres-Carrasco, M. Use of glass waste as an activator in the preparation of alkali-activated slag. Mechanical strength and paste characterisation. *Cem. Concr. Res.* **2014**, *57*, 95–104. [CrossRef]
33. Dung, N.; Hooper, T.; Unluer, C. Accelerating the reaction kinetics and improving the performance of Na_2CO_3-activated GGBS mixes. *Cem. Concr. Res.* **2019**, *126*, 105927. [CrossRef]
34. Chen, Y.; Wu, X.; Yin, W.; Tang, S.; Yan, G. Effects of Waste Glass Powder on Rheological and Mechanical Properties of Calcium Carbide Residue Alkali-Activated Composite Cementitious Materials System. *Materials* **2023**, *16*, 3590. [CrossRef]
35. Shen, J.; Li, Y.; Lin, H.; Li, Y. Development of autogenous shrinkage prediction model of alkali-activated slag-fly ash geopolymer based on machine learning. *J. Build. Eng.* **2023**, *71*, 106538. [CrossRef]
36. Zanotti, C.; Borges, P.H.; Bhutta, A.; Banthia, N. Bond strength between concrete substrate and metakaolin geopolymer repair mortar: Effect of curing regime and PVA fiber reinforcement. *Cem. Concr. Compos.* **2017**, *80*, 307–316. [CrossRef]
37. Kianynejad, M.; Toufigh, M.M.; Toufigh, V. Mechanical Performance of Alkali-activated Stabilized Sandy Soil Reinforced with Glass Wool Residue Microfibers. *KSCE J. Civ. Eng.* **2024**, *28*, 581–595. [CrossRef]
38. Xia, M.; Muhammad, F.; Zeng, L.; Li, S.; Huang, X.; Jiao, B.; Shiau, Y.; Li, D. Solidification/stabilization of lead-zinc smelting slag in composite based geopolymer. *J. Clean. Prod.* **2019**, *209*, 1206–1215. [CrossRef]
39. An, Y.C.; Liu, Q.; Tan, B.; He, H. Experimental Study on Preparation of Pavement Base Material by Coordination of Red Mud, Steel Slag and Cement. *J. Highw. Transp. Res. Dev.* **2023**, *40*, 35–43.
40. Guo, X.; Huang, J. Effects of Cr^{3+}, Cu^{2+}, and Pb^{2+} on Fly Ash based Geopolymer. *J. Wuhan Univ. Technol. Sci. Ed.* **2019**, *34*, 851–857. [CrossRef]
41. Liu, Z.; Li, L.; Zhang, Y.; Wang, D. Immobilization of Heavy Metal Pb2+ Using Fly Ash Based Geopolymer. *Bull. Chin. Ceram. Soc.* **2018**, *37*, 1382–1386.
42. Guo, X.L.; Zhang, L.Y.; Shi, X.S. Effect factors and mechanism of solidification/stabilization of heavy metals by geopolymers. *J. Funct. Mater.* **2015**, *46*, 5013–5018.
43. *GB/T 17671-2021*; Test Method of Cement Mortar Strength (ISO Method) (ISO 679:2009, Cement—Test Methods—Determination of Strength, MOD). China National Standardization Administration Committee: Beijing, China, 2021.
44. *JTG E51-2009*; Test Methods of Materials Stabilized with Inorganic Binders for Highway Engineering. Ministry of Transport of the People's Republic of China: Beijing, China, 2010.
45. Wang, Q.; Wang, Y.; Gu, X.; Liu, J.; Xu, X. Study on the Properties and Hydration Mechanism of Calcium Carbide Residue-Based Low-Carbon Cementitious Materials. *Buildings* **2024**, *14*, 1259. [CrossRef]
46. *JTGT F20-2015*; Technical Guidelines for Construction of Highway Roadbases. Ministry of Transport of the People's Republic of China: Beijing, China, 2015.
47. Shao, J.; Gao, J.; Zhao, Y.; Chen, X. Study on the pozzolanic reaction of clay brick powder in blended cement pastes. *Constr. Build. Mater.* **2019**, *213*, 209–215. [CrossRef]
48. Wu, M.; Zhang, Y.; Jia, Y.; She, W.; Liu, G.; Yang, Z.; Zhang, Y.; Zhang, W.; Sun, W. Effects of sodium sulfate on the hydration and properties of lime-based low carbon cementitious materials. *J. Clean. Prod.* **2019**, *220*, 677–687. [CrossRef]
49. Sun, C.; Zhang, J.; Yan, C.; Yin, L.; Wang, X.; Liu, S. Hydration characteristics of low carbon cementitious materials with multiple solid wastes. *Constr. Build. Mater.* **2022**, *322*, 126366. [CrossRef]
50. Zhang, N.; Li, H.; Liu, X. Hydration mechanism and leaching behavior of bauxite-calcination-method red mud-coal gangue based cementitious materials. *J. Hazard. Mater.* **2016**, *314*, 172–180. [CrossRef]
51. Guo, W.; Zhang, Z.; Zhao, Q.; Song, R.; Liu, J. Mechanical properties and microstructure of binding material using slag-fly ash synergistically activated by wet-basis soda residue-carbide slag. *Constr. Build. Mater.* **2021**, *269*, 121301. [CrossRef]
52. Temuujin, J.; van Riessen, A.; Williams, R. Influence of calcium compounds on the mechanical properties of fly ash geopolymer pastes. *J. Hazard. Mater.* **2009**, *167*, 82–88. [CrossRef]